1.2 RECENT OBSERVATIONS OF HELIUM EFFECTS ON CAVITY EVOLUTION IN TEMPERED MARTENSITIC STEELS

— T. Yamamoto, Y. Wu, G. R. Odette, (University of California, Santa Barbara); S. Kondo, and A. Kimura (Kyoto University)

OBJECTIVE

The objective of this work is to characterize the effects of He/dpa ratio on cavity evolution under Fe^{3+} and He^{+} dual ion beam irradiation in a normalized and tempered martensitic steel (TMS) F82H mod.3.

SUMMARY

New dual ion (Fe^{3+} and He^{+}) beam irradiations (DII) were performed at 500°C on a group of ferritic alloys up to nominal dpa and He levels of 26 dpa and 390 appm, respectively, at a He (appm)/dpa ratio of ≈ 15 using the DuET facility at Kyoto University in Japan. The actual dpa, He and He/dpa vary with depth in the sample. The alloys studied include normalized and tempered martensitic steels, (TMS) F82H IEA in as-tempered and cold-worked conditions as well as F82H mod.3, and a nanostructured ferritic alloy (NFA), MA957. To date, TEM observations have been performed for F82H mod.3 at depths from 0.1 to 1.7 mm. In the F82H mod.3, the number density of the cavities (N) ranged from 1 to 9 x $10^{21}/m^3$ while average diameter (<d>) of all the cavities ranged from 2.4 to 5.5 nm. The N are significantly smaller than that for higher ≈ 47 appm He/dpa in previous study, while the <d> are similar.

BACKGROUND

Predicting and mitigating the effects of a combination of large levels of transmutant He and displacement damage (dpa), produced by high energy neutrons, on the dimensional stability and mechanical properties of structural materials is one of the key challenges in the development of fusion energy [1]. The fundamental overriding questions about He-dpa synergisms include: a) what are the basic interacting mechanisms controlling He and defect transport, fate and consequences, and how are they influenced by the starting microstructure and irradiation variables (dpa rate, He/dpa ratio, temperature and applied stress) and, b) how can the detrimental effects of He-dpa synergisms be mitigated and managed by proper microstructural design? In the absence of a fusion neutron source, we have been utilizing various alternative experimental techniques to study the He-dpa synergisms, that includes: a) in situ He implantation (ISHI) in mixed spectrum fission reactors, HFIR at ORNL and ATR at INL; b) spallation proton irradiation (SPI) in STIP (spallation target irradiation projects) at Paul Sherr Institute in Switzerland; and, c) multiple ion beams to simultaneously implant He and create displacement damage with heavy ions. In this work we specifically use the dual ion beam irradiation (DII) facility, DuET, at Kyoto University, Japan. The DII produces a broad range of dpa and He up to very high levels in short periods of time. However, great caution is required in applying DII data to neutron irradiation conditions due to a host of differences including dpa rates, the proximity of a free surface and injected interstitials and impurities in some cases. Nevertheless, DII are useful for mechanism studies and it is important to compare and contrast DII microstructural evolutions with the corresponding effects of neutron irradiations. Here we report the results of DII up to ≈ 45 dpa at He/dpa ratio of ≈ 15 appm/dpa compared with our earlier results for He/dpa ≈ 47 appm/dpa [2].

PROGRESS AND STATUS

Experimental Procedure

Table 1 summarizes the irradiation conditions of our new and previous DII experiments performed on ferritic materials at 500 °C. The new irradiation was aimed to achieve the same nominal displacement damage level of 26 dpa as in a previous study, but at a lower, 15 versus 47, appm He/dpa ratio. The alloys included were F82H IEA in as tempered as well as in 20% or 50% cold-worked conditions, F82H mod.3 and MA957. The latter two alloys are common to all irradiation conditions and permit single variable comparisons. The irradiated specimens, with mechanically and electrically polished surfaces, were in the form of coupons approximately 1 mm wide and 20 mm long extracted from 0.5 mm thick wafers. The DII was performed in DuET facility at the Institute of Advanced Energy, Kyoto University (Kyoto, Japan). The Fe^{3+} ions were accelerated to 6.4MeV by a tandem accelerator and the He^{+} ions were accelerated to 1MeV by a single end accelerator. The specimens were positioned in a temperature-monitored/controlled stage. The He^{+} ion beam passed through a rotating energy degrader creating four ion implantation energy bands that result in a broader and more uniform He deposition profile up to the maximum depth of ≈ 1.5 mm. Figure 1a shows dpa and He profiles estimated using TRIM 2008 code for ion currents that were monitored and re-adjusted hourly. The damage calculations are based on Kinchin-Pease model with displacement energies of 40 eV for Fe and Cr as recommended in ASTM E521-96 (2009) [3]. The displacement damage increases with depth to peak at ≈ 1.5 mm deep and tails off at ≈ 2 mm deep. The overall He profile created by four energy bands has a slightly smaller range. The He deposition increases within the range from ≈ 400 appm at 0.4 mm to ≈ 670 appm at 1.1 mm deep, roughly tracking the corresponding dpa. Thus the resulting He/dpa ratio is relatively constant at 16.3 ± 2.4 appm/dpa over a wide depth interval. Figure 1b shows the corresponding estimates for the previous irradiation that had ≈ 3 times more He with almost identical dpa damage levels.

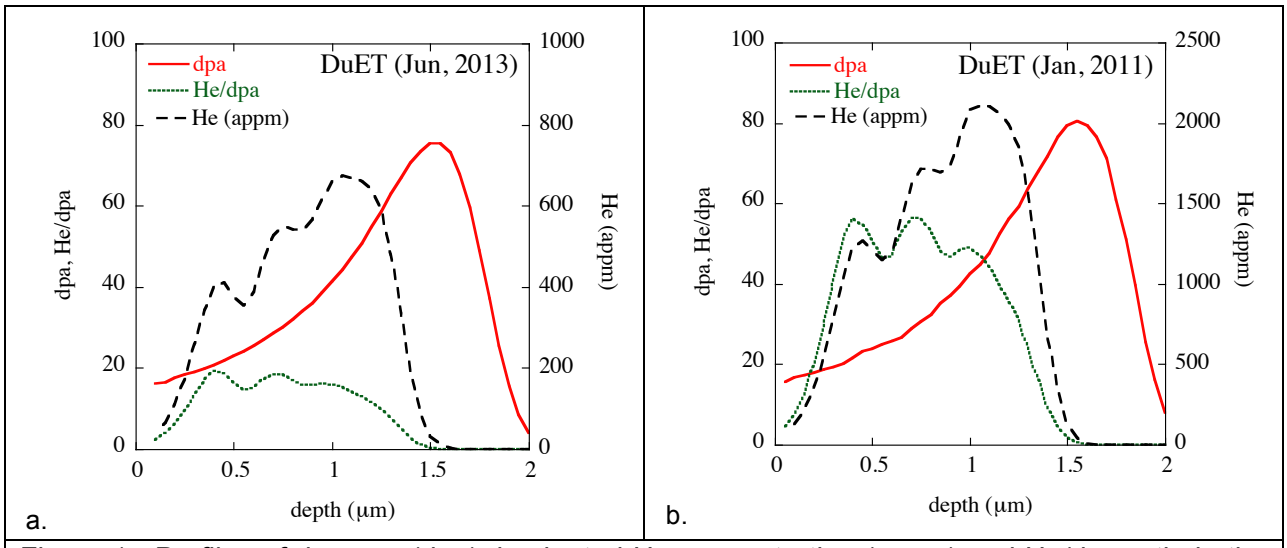

Figure 1. Profiles of damage (dpa), implanted He concentration (appm) and He/dpa ratio in the (a) new and (b) previous dual ion irradiations.

A FEI HELIOS Focused Ion Beam (FIB) tool was used to micro-machine < 100 nm thick electron transparent ≈ 5 μm wide and 5 μm deep lift-outs that included both damaged-implanted and undamaged regions. TEM was performed on the FEI 200 keV Technai T20 and 300 KeV Titan instruments in the UCSB Microstructure and Microanalysis Facility. Through focus series images were analyzed to identify and quantify the average diameter (<d>), number density (N) and volume fraction (f_v) of cavities at various depths.

Table 1. Summary of DuET experimental conditions.

Exp ID	Materials	T (°C)	Nominal Condition (@550-650nm)				Peak He (@1000-1100nm)		
			dpa	He (appm)	He/dpa	dpa/s	dpa	He (appm)	He/dpa
DI10B1	F82H mod.3, MA957	500	26	1210	47	5.0×10^{-4}	45	2100	47
DI10B3			10	480	47	5.1×10^{-4}	18	840	47
DI13A1	F82H mod.3, F82H IEA (AT, 20%CW or 80%CW), MA957	500	26	390	15	5.1×10^{-4}	44	670	15

Results

Cavity Microstructures After DII at 500°C

Figure 2 compares low magnification overviews of representative cavity microstructure over the depth range from 0 to 2 μm for a) 15 appm He/dpa and b) 47 appm He /dpa, in the images taken at -1500 nm underfocus condition. The cavity formation peaks near the highest He concentration at the depth around 1.1 μm in both cases. Cavity formation can also be seen near the surface at a depth as shallow as ≈ 0.02 μm at corresponding damage level of ≈ 5 dpa and He levels of ≈ 10 appm and ≈ 30 appm, respectively. Cavity formation is also observed up to a depth of ≈ 1.75 μm in 15 appm He/dpa case and up to 1.63 μm in 47 appm He/dpa case. This corresponds to the maximum He energy/range in the DII irradiation. These general trends are consistent to the evaluation of implanted He concentrations shown in Figs 1.

Figure 3 compares higher magnification cavity images in the peak He region for both He/dpa conditions. The depth increases from top to bottom and the estimated dpa levels are ≈ 45 dpa at the center of the images; the corresponding He concentrations are 670 (Figure 3a) appm and 2100 (Figure 3b) appm, respectively. Clearly the higher He creates significantly more visible cavities. However, even in the lower He case most of the cavities appear to have transformed to growing faceted voids with a peak at sizes that are similar to those in the higher He case. Figure 4 shows the size distribution of cavities, including data from other locations at the same depth. Three quarters of cavities are around 6.5 nm in diameter in the lower He case, with a peak that is shifted to a larger size than for the higher He/dpa case, at ≈ 4 nm in the latter case; however voids as large as ≈ 20 nm in diameter are observed in higher He condition. Note, due to the small N, from ≈ 0.7 to 8.6 $\times 10^{21}/m^3$, at lower He, far fewer cavities sampled, even though the same total area of the sample was imaged. We will continue to analyze the lower He/dpa case to get a better statistics on the cavity size distributions.

Figure 5a shows the <d> of cavities obtained in 100 nm sections over the entire implantation depth range from 0.1 to 1.6 μm in the sample DII at both appm He/dpa. Figures 5b and 5c shows the corresponding cavity N and f, respectively. The N is fewer in at the lower He/dpa, but the <d> are remarkably similar. The corresponding f_v is much lower than in the higher He case, due to the large difference in N.

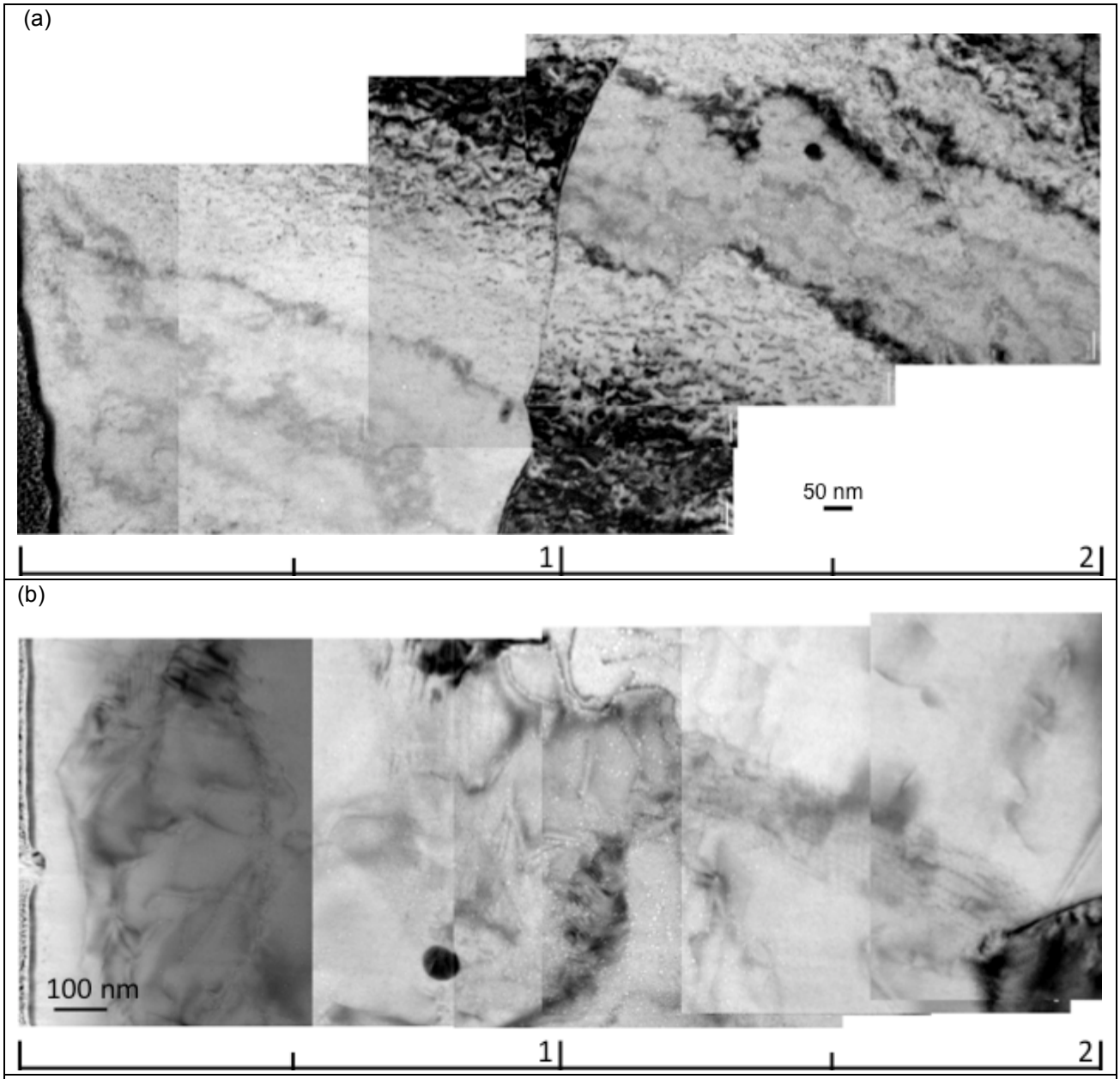

Figure 2. Overview of TEM cavity images in the depth range from 0 to 2 mm in F82H mod.3 DI irradiated at 500 °C to nominally a) 26 dpa and 390 appm He and, b) 26 dpa and 1210 appm He.

Discussion

In our previous analyses of DuET and HFIR in-situ helium implantation (ISHI) experiments, He*dpa was used as an add-hoc but useful parameter to view data trends in the various He and dpa conditions. Figures 6 show the updated plots of <d>, N and f_v as a function of He*dpa for most of the data obtained in our DuET and ISHI experiments in the TMS alloys including Eurofer 97 and F82H mod.3 in cold-worked condition. Note that the cavity statistics are very sensitive to the local microstructure, which varies significantly from place to place. Thus the variability in comparing small regions of irradiated volume is very large. Since the ISHI regions are order 25 or larger than for the DII, the variability in the latter case is especially significant. Thus the shaded regions in Figure 6 are meant to draw attention to general trends that have been observed. Additional TEM studies that cross-correlate local microstructure characteristics with cavity statistics will be needed for further quantification. The average cavity size, <d>, increases with He*dpa and is similar for the ISHI and DII conditions. The cavity number density, N, appears to peak in both cases and on average is much higher for the ISHI case, especially compared to the lower He DII condition. The cavity volume fraction, f_v, increases more rapidly for the ISHI, beginning at a lower He*dpa.

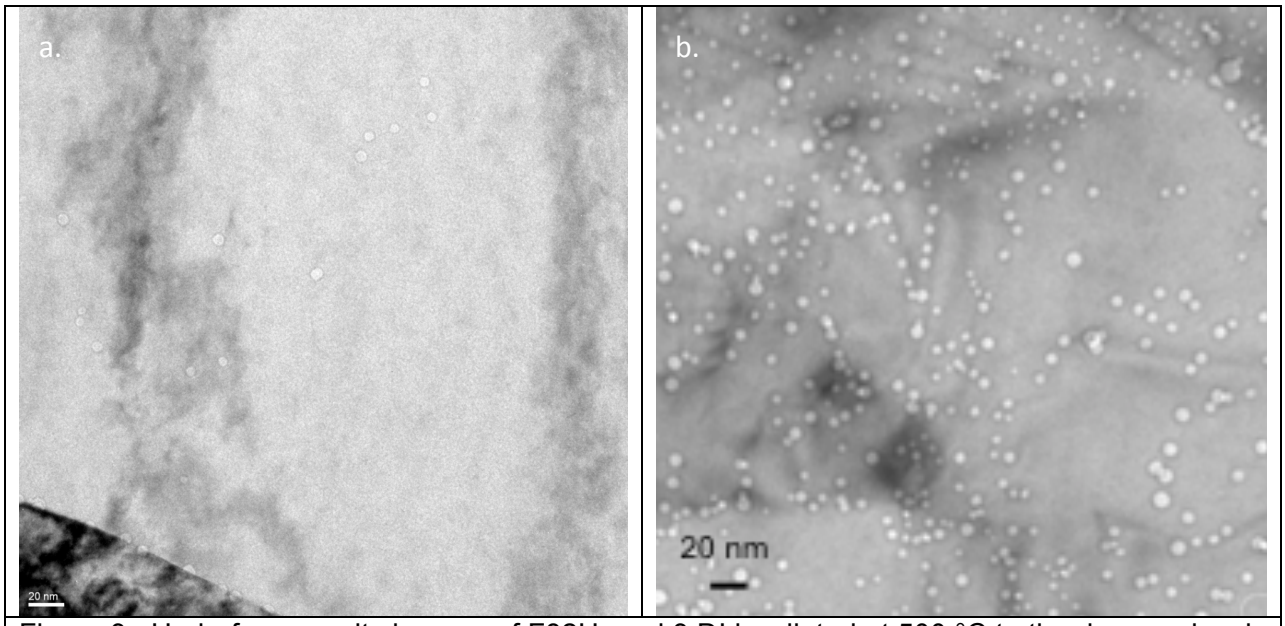

Figure 3. Underfocus cavity images of F82H mod.3 DI irradiated at 500 °C to the damage level of ≈ 45 dpa and He levels of (a) 670 appm and (b) 2100 appm. The damage and He levels are estimated for the vertically center location in the images.

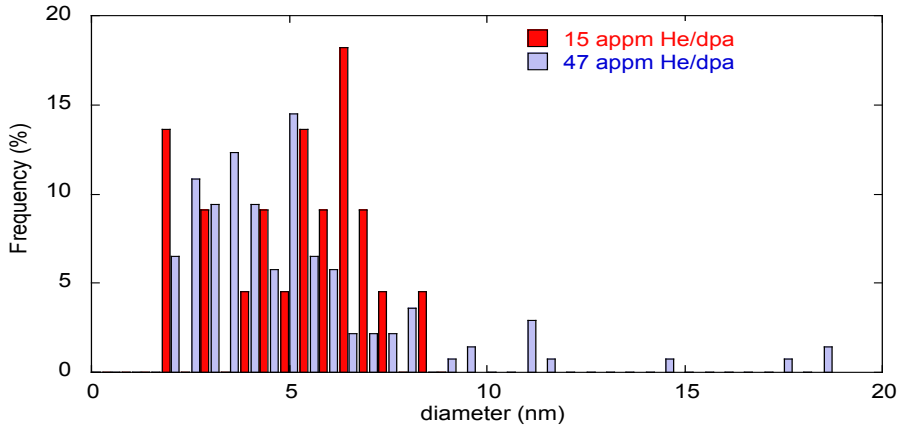

Figure 4. Size distributions of cavities in F82H mod.3 DI irradiated at 500 °C to the damage level of ≈ 45 dpa and He levels of 670 appm and 2100 appm. The damage and He levels are estimated at the center depth location of the images.

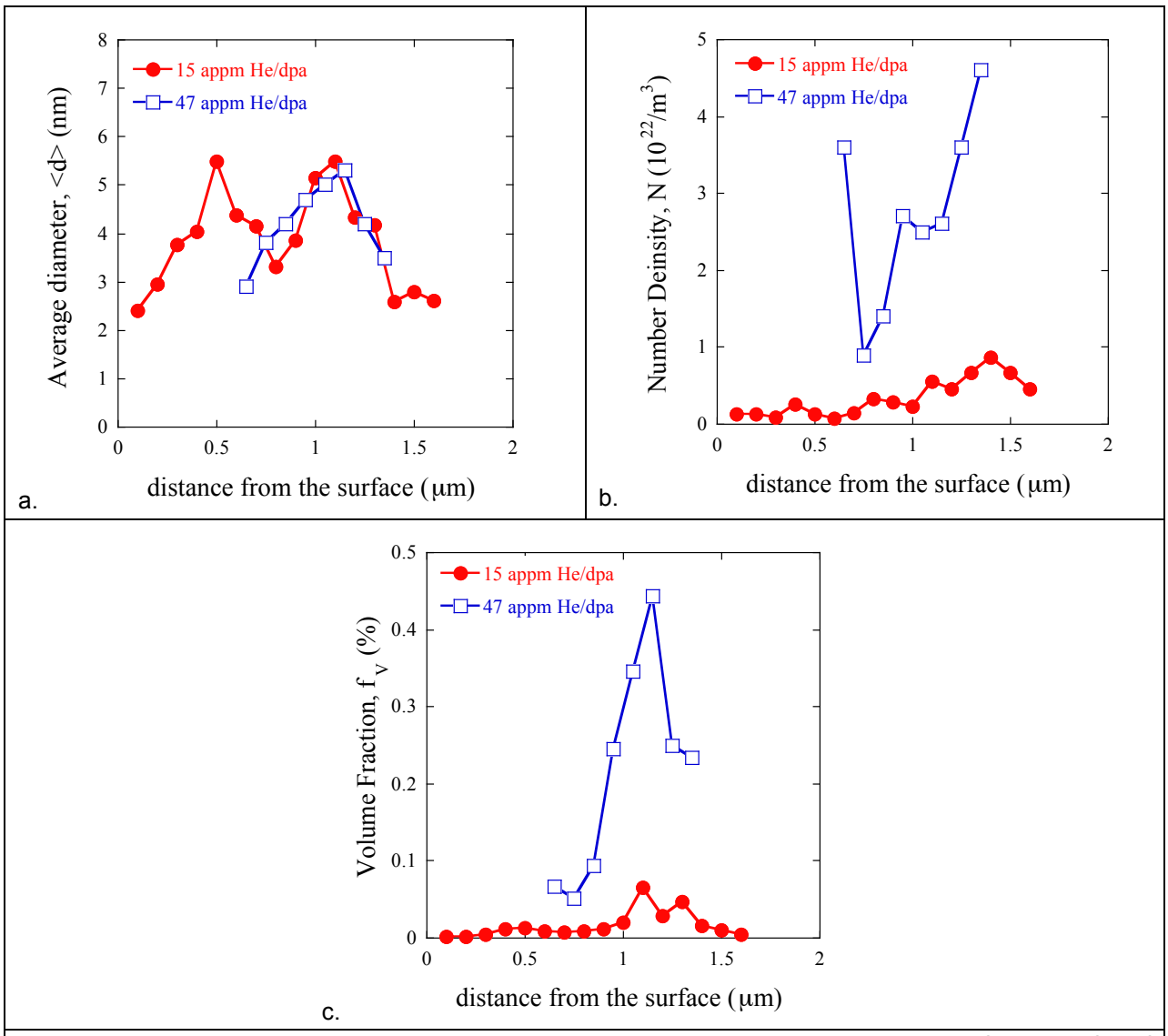

Figure 5. a) Average diameter (<d>), b) number density (N) and c) volume fraction (f_v) of cavities in F82H mod.3 DI irradiated at 15 or 47 appm He/dpa, as a function of depth from surface.

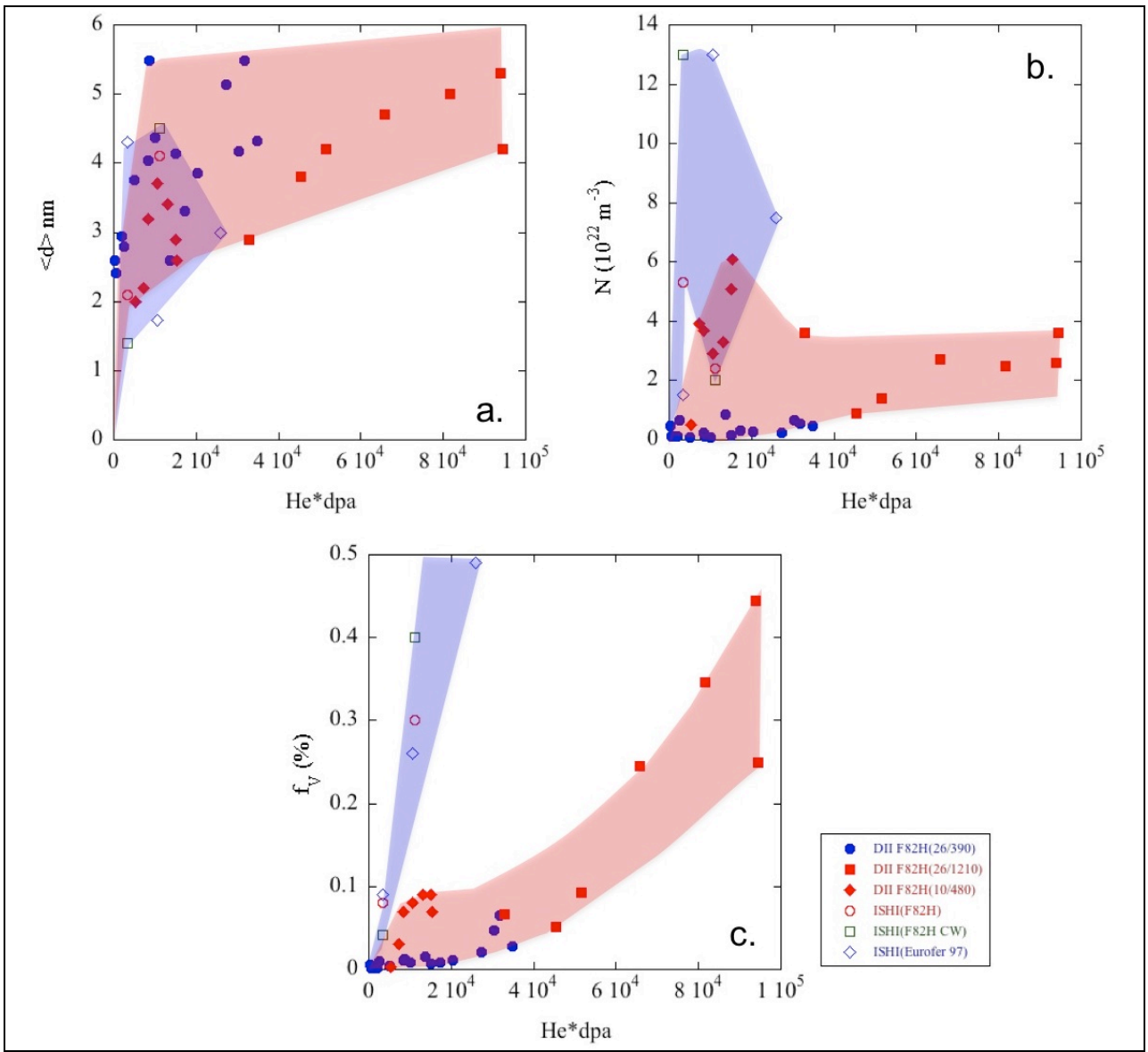

Figure 6. a) Average diameter (<d>), b) number density (N) and c) volume fraction (f_v) of cavities in TMS alloys DII or ISHI as a function of He * dpa.

FUTURE WORK

We will continue to analyze microstructures from previous a new DII experiments.

ACKNOWLEDGEMENTS

The work performed at UCSB was supported by the U. S. Department of Energy, Office of Fusion Energy Sciences, under contract DE-FG03-94ER54275. The DuET experiments are supported by the Joint Usage/Research Program on Zero-Emission Energy Research, Institute

of Advanced Energy, Kyoto University. We acknowledge the contributions of the NSF sponsored UCSB Microstructure and Microanalysis Facility.

REFERENCES

[1] Y. Dai, G. R. Odette, and T. Yamamoto, "*The Effects of helium on irradiated structural alloys," in Comprehensive Nuclear Materials, R. Konings, T. R. Allen, R. E. Stoller, and S. Yamanaka Eds. (2012) Elsevier.*
[2] T. Yamamoto, Y. Wu, G. R. Odette, K. Yabuchi, S. Kondo, and A. Kimura, *Fusion Materials Semiannual Report 12/31/2010* DOE/ER-313/52 (2011) 8.
[3] ASTM Standards E521-96 (2009), ASTM International (2009).